Response of a Cylindrical Shell with Finite Length Ring Stiffeners

Andrew J. Hull

Undersea Warfare Weapons, Vehicles and Defensive Systems Department, Naval Undersea Warfare Center Division, Newport, Rhode Island 02841 USA

Geoffrey R. Moss

Sensors and Sonar Systems Department, Naval Undersea Warfare Center Division, Newport, Rhode Island 02841 USA

(Received 24 September 2014; accepted 19 April 2016)

This paper derives a spatial domain wave propagation solution of a cylindrical shell that contains periodically spaced ring stiffeners. Previous work in this area has modeled the stiffeners as having a very short or very long length. This paper models the stiffeners as finite length inclusions with forces that have spatial extent in three-dimensions. Furthermore, there is a well-defined separation distance between each stiffener. The new model uses Donnell shell equations with the stiffener forces applied in three-dimensions using Heaviside step functions. These equations of motion are orthogonalized in both the angular and longitudinal directions, resulting in a double fixed index matrix equation. These indices can be varied, which yields a set of double indexed matrix equations that are written together as a single global matrix. This global matrix can be solved, which results in a solution to the system displacements. Two specific external loading cases are investigated and convergence criteria are discussed. One of the models is verified with a comparison to finite element analysis.

1. INTRODUCTION

Reinforced shells were used in a variety of applications. They can be found in undersea vehicles, industrial pipes, hydraulic lines, and marine piers. Reinforcement was typically added to these structures as a method to increase stiffness without adding significant mass. Adding reinforcement changes the structural response of almost any system, and the forces that are introduced by the reinforcement need to be included in an analytical or numerical model that predicts the corresponding response. Unreinforced isotropic thin cylindrical shell models have existed in the literature for a long time and can be found in textbooks on acoustics and applied mechanics.[1,2] Isotropic thick shell cylindrical shells models were also derived for shells without reinforcement.[3] Shell models were extended to include transversely isotropic behavior[4] and general orthotropic behavior.[5]

The inclusion of ring stiffeners in the cylinder increased the stiffness in all three cylindrical directions and changed the character of the infinite cylinder response from a (purely propagating) single longitudinal term expression to a (partially reflective) multi-longitudinal term expression due to the forces of the stiffeners interacting with the wave motion. Historically, research in this area has been divided into two separate approaches: (1) where the length of the stiffener was very short compared to the periodicity of the stiffeners or (2) where the length of the stiffener was relatively long compared its periodicity. Work in the first area (i.e. short stiffeners) was abundant, and various systems were analyzed. Free wave propagation of periodically ring stiffened shells has been studied using finite element analysis[6] applied to various different ring geometries that all had relatively small spatial extent and to determine natural frequencies and modes shapes of ring-stiffened shells.[7] The free vibration analysis of cylindrical shells with ring stiffeners that had non-uniform eccentricity and unequal spacing were investigated using a Ritz analytical method, experimental testing, and finite element analysis,[8] where the stiffeners had a relatively small spatial extent.

A Laplace transfer numerical method to analyze ring stiffened circular thin shells was developed,[9] where the spatial dimensions of the rings were small and the structure was loaded with a transient pressure load. The problem of acoustic radiation from fluid-loaded, ring-supported thin shells subjected to a point forces has been solved[10] in the wavenumber domain. In this paper, both single and double periodic ring supports were considered. The theory of vibrations of a cylinder reinforced by periodically spaced circular T-section ribs along its length has been derived.[11] A method for obtaining the propagation constants of a thin uniform periodically stiffened cylindrical shells with an emphasis on the stop and pass bands of free wave motion has been developed.[12]

Work in the second area (i.e. long stiffeners) generally used wave propagation approaches to model finite length ring-stiffened cylindrical shells by assuming that the structure behaves as an orthotropic shell, a method that is sometimes referred to as "smearing". This was studied for initial hydrostatic pressure using Flugge equations of motion[13] and for fi-

nite length structures with arbitrary boundary conditions with an axial factor term analysis.[14] The effects of energy reflections off of the stiffener edges were absent in these two papers, although these models captured the majority of the wave propagation features of such a system.

This paper derived a spatial domain wave propagation solution for the problem of a cylindrical shell with periodically spaced ring stiffeners that had a significant spatial extent and significant separation. This model was designed to bridge the gap between previous models, where the stiffeners were modeled as extremely short or extremely long. The problem began with the Donnell shell equations of motion written with the stiffener forces applied in three-dimensions using Heaviside step functions. The shell displacements were written as double summations of an unknown wave propagation coefficient multiplied by an indexed circumferential term multiplied by an indexed longitudinal term. The displacement terms were inserted into the differential equations of motion and the Heaviside functions were approximated by a Fourier series. These algebraic equations were then orthogonalized in two spatial dimensions, which resulted in a matrix equation that was dependent on two fixed indices: one an angular index and the other a longitudinal index. By using a finite number of these indices, the fixed index matrix equations were assembled into a global matrix equation, which resulted in a solution to the wave propagation coefficients. By using these coefficients, the displacement field of the shell could be calculated. This problem was investigated for two external forcing conditions: one a ring load and the other a plane wave load. The ring load was verified by comparing the results to a solution generated using finite element theory. Convergence criteria were discussed and the energy distribution of the different mode numbers was investigated.

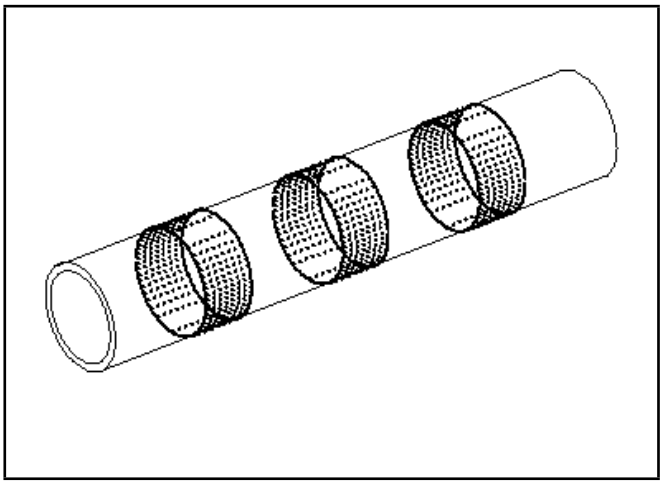

Figure 1. Isometric view of the cylinder with ring stiffeners.

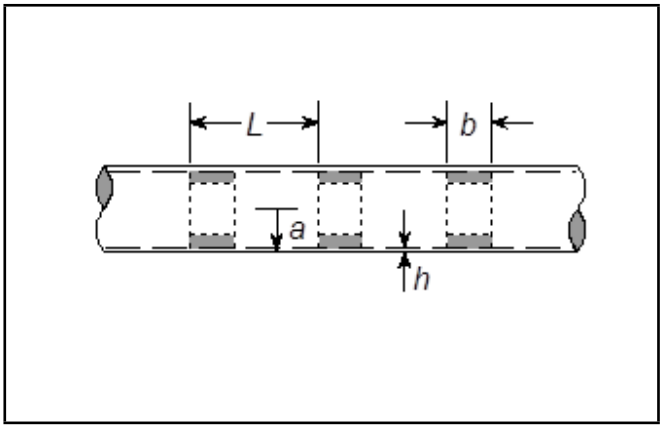

Figure 2. Side view of the cylinder with ring stiffeners.

2. SYSTEM MODEL AND DECOUPLED SOLUTION

The system model was that of a cylinder containing a radial stiffener of finite length, as shown in Figs. 1 and 2. This problem was analytically modeled by assuming the cylinder was governed with a dynamic formulation of Donnell shell equations and the stiffener was modeled as a spatially distributed translational spring in the longitudinal, circumferential, and radial directions. The model used the following assumptions: (1) the cylinder had infinite spatial extent in the axial direction, (2) the displacements in the cylinder were three-dimensional and linear, (3) the displacement field was constant across the thickness of the shell, (4) the stiffeners were periodic, and (5) the stiffener exerted forces in the longitudinal, circumferential, and radial directions on the cylinder that were proportional to the longitudinal, circumferential, and radial displacements of the cylinder, respectively.

The motion of the cylinder with ring stiffeners was governed by the equation of motion in the longitudinal direction written as:

$$\rho h\frac{\partial^2 u(z,\theta,t)}{\partial t^2} - \rho h c_p^2\frac{\partial^2 u(z,\theta,t)}{\partial z^2} - \frac{(1-\nu)\rho h c_p^2}{2a^2}\frac{\partial^2 u(z,\theta,t)}{\partial \theta^2} - \frac{(1+\nu)\rho h c_p^2}{2a}\frac{\partial^2 v(z,\theta,t)}{\partial z\partial\theta} - \frac{\nu\rho h c_p^2}{a}\frac{\partial w(z,\theta,t)}{\partial z} = \frac{K_z}{ab}u(z,\theta,t)\sum_{n=-\infty}^{n=+\infty}\left[\mathrm{H}(z-nL)-\mathrm{H}(z-b-nL)\right]; \quad (1)$$

in the tangential direction written as:

$$-\frac{(1+\nu)\rho h c_p^2}{2a}\frac{\partial^2 u(z,\theta,t)}{\partial z\partial\theta} - \frac{(1-\nu)\rho h c_p^2}{2}\frac{\partial^2 v(z,\theta,t)}{\partial z^2} - \frac{\rho h c_p^2}{a^2}\frac{\partial^2 v(z,\theta,t)}{\partial\theta^2} + \rho h\frac{\partial^2 v(z,\theta,t)}{\partial t^2} - \frac{\rho h c_p^2}{a^2}\frac{\partial w(z,\theta,t)}{\partial\theta} = \frac{K_t}{ab}v(z,\theta,t)\sum_{n=-\infty}^{n=+\infty}\left[\mathrm{H}(z-nL)-\mathrm{H}(z-b-nL)\right]; \quad (2)$$

and in the radial direction written as:

$$\frac{\nu\rho hc_p^2}{a}\frac{\partial u(z,\theta,t)}{\partial z}+\frac{\rho hc_p^2}{a^2}\frac{\partial v(z,\theta,t)}{\partial \theta}+\frac{\rho hc_p^2}{a^2}w(z,\theta,t)+\frac{\rho h^3c_p^2}{12}\frac{\partial^4 w(z,\theta,t)}{\partial z^4}+\frac{\rho h^3c_p^2}{6a^2}\frac{\partial^4 w(z,\theta,t)}{\partial z^2\partial\theta^2}+\frac{\rho h^3c_p^2}{12a^4}\frac{\partial^4 w(z,\theta,t)}{\partial\theta^4}+\rho h\frac{\partial^2 w(z,\theta,t)}{\partial t^2}=p_a(z,\theta,t)+\frac{K_r}{ab}w(z,\theta,t)\sum_{n=-\infty}^{n=+\infty}\left[\mathrm{H}(z-nL)-\mathrm{H}(z-b-nL)\right]; \quad (3)$$

where z was the axial direction, θ was the circumferential direction, t was time, $u(z,\theta,t)$ was the longitudinal displacement, $v(z,\theta,t)$ was the tangential displacement, $w(z,\theta,t)$ was the radial displacement, a was the radius of the shell, ν was Poisson's ratio of the shell, ρ was the density of the shell, h was the thickness of the shell, $p_a(z,\theta,t)$ was the external radial load on the shell, K_z as the longitudinal stiffness of the ring stiffener, K_t was the circumferential stiffness of the ring stiffener, K_r as the radial stiffness of the ring stiffener, b was the length of the ring stiffener, $\mathrm{H}(\cdot)$ was the Heaviside step function, and c_p was the plate wave speed, which was given by:

$$c_p=\sqrt{\frac{E}{\rho(1-\nu^2)}}. \quad (4)$$

The shell displacements were then written as double summations in the form:

$$u(z,\theta,t)=\sum_{m=-\infty}^{m=+\infty}\sum_{q=0}^{q=+\infty}U_{mq}\cos(q\theta)\exp(\mathrm{i}k_m z)\exp(-\mathrm{i}\omega t); \quad (5)$$

$$v(z,\theta,t)=\sum_{m=-\infty}^{m=+\infty}\sum_{q=0}^{q=+\infty}V_{mq}\sin(q\theta)\exp(\mathrm{i}k_m z)\exp(-\mathrm{i}\omega t); \quad (6)$$

and

$$w(z,\theta,t)=\sum_{m=-\infty}^{m=+\infty}\sum_{q=0}^{q=+\infty}W_{mq}\cos(q\theta)\exp(\mathrm{i}k_m z)\exp(-\mathrm{i}\omega t); \quad (7)$$

where i was the square root of -1, ω was the frequency, U_{mq} , V_{mq} , and W_{mq} were unknown longitudinal, tangential, and radial wave propagation coefficients respectively, whose solutions were sought, and k_m was the indexed longitudinal wavenumber, which was expressed as:

$$k_m=k+\frac{2\pi m}{L}; \quad (8)$$

where k was the wavenumber of excitation and L was the periodic spacing of the ring stiffeners. For the problems solved in this paper, the excitation was a ring load at definite wavenumber and frequency written as:

$$p_a(z,\theta,t)=P_a\exp(\mathrm{i}kz)\exp(-\mathrm{i}\omega t); \quad (9)$$

or a broad side plane wave at definite speed and frequency written as:

$$p_a(z,\theta,t)=P_a\left[\sum_{n=0}^{n=+\infty}\mathrm{i}^n\varepsilon_n\mathrm{J}_n\left(\frac{\omega a}{c}\right)\cos(n\theta)\right]\exp(-\mathrm{i}\omega t); \quad (10)$$

where P_a was the magnitude of the applied pressure excitation, ϵ_n was the Newmann factor ($\epsilon_n=1$ for $n=0$; $\epsilon_n=2$ for $n>0$), J was an ordinary nth order Bessel function of the first kind, and c was the propagation speed of the plane wave. At this point, the exponential with respect to time was suppressed in all of the equations. The insertion of Eqs. (5) to (9) into Eqs. (1) to (3) yielded:

$$\sum_{m=-\infty}^{m=+\infty}\sum_{q=0}^{q=+\infty}\left[\rho hc_p^2k_m^2+\frac{\rho hc_p^2(1-\nu)q^2}{2a^2}-\rho h\omega^2\right]\times U_{mq}\cos(q\theta)\exp(\mathrm{i}k_m z)+\sum_{m=-\infty}^{m=+\infty}\sum_{q=0}^{q=+\infty}\left[\frac{-\rho hc_p^2(1+\nu)\,\mathrm{i}\,k_m q}{2a}\right]\times V_{mq}\cos(q\theta)\exp(\mathrm{i}k_m z)+\sum_{m=-\infty}^{m=+\infty}\sum_{q=0}^{q=+\infty}\left[\frac{-\rho hc_p^2\nu\,\mathrm{i}\,k_m}{a}\right]W_{mq}\cos(q\theta)\exp(\mathrm{i}k_m z)=\frac{K_z}{ab}\sum_{m=-\infty}^{m=+\infty}\sum_{q=0}^{q=+\infty}U_{mq}\cos(q\theta)\exp(\mathrm{i}k_m z)\times\sum_{n=-\infty}^{n=+\infty}\left[\mathrm{H}(z-nL)-\mathrm{H}(z-b-nL)\right]; \quad (11)$$

$$\sum_{m=-\infty}^{m=+\infty}\sum_{q=0}^{q=+\infty}\left[\frac{\rho hc_p^2(1+\nu)\,\mathrm{i}\,k_m q}{2a}\right]\times U_{mq}\sin(q\theta)\exp(\mathrm{i}k_m z)+\sum_{m=-\infty}^{m=+\infty}\sum_{q=0}^{q=+\infty}\left[\frac{\rho hc_p^2(1-\nu)k_m^2}{2}+\frac{\rho hc_p^2q^2}{a^2}-\rho h\omega^2\right]\times V_{mq}\sin(q\theta)\exp(\mathrm{i}k_m z)+\sum_{m=-\infty}^{m=+\infty}\sum_{q=0}^{q=+\infty}\left[\frac{\rho hc_p^2\,q}{a^2}\right]W_{mq}\sin(q\theta)\exp(\mathrm{i}k_m z)=\frac{K_t}{ab}\sum_{m=-\infty}^{m=+\infty}\sum_{q=0}^{q=+\infty}V_{mq}\sin(q\theta)\exp(\mathrm{i}k_m z)\times\sum_{n=-\infty}^{n=+\infty}\left[\mathrm{H}(z-nL)-\mathrm{H}(z-b-nL)\right]; \quad (12)$$

and

$$\sum_{m=-\infty}^{m=+\infty}\sum_{q=0}^{q=+\infty}\left[\frac{\rho h c_p^2 \nu \,\mathrm{i}\, k_m}{a}\right] U_{mq}\cos(q\theta)\exp(\mathrm{i}k_m z)+ \sum_{m=-\infty}^{m=+\infty}\sum_{q=0}^{q=+\infty}\left[\frac{\rho h c_p^2\, q}{a^2}\right] V_{mq}\cos(q\theta)\exp(\mathrm{i}k_m z)+ \sum_{m=-\infty}^{m=+\infty}\sum_{q=0}^{q=+\infty}\left[\frac{\rho h c_p^2}{a^2}+\frac{\rho h^3 c_p^2 k_m^4}{12}+\frac{\rho h^3 c_p^2 k_m^2 q^2}{6a^2}+ \frac{\rho h^3 c_p^2 q^4}{12a^4}-\rho h\omega^2\right] W_{mq}\cos(q\theta)\exp(\mathrm{i}k_m z) = P_a\exp(\mathrm{i}kz)+\frac{K_r}{ab}\sum_{m=-\infty}^{m=+\infty}\sum_{q=0}^{q=+\infty} W_{mq}\cos(q\theta)\exp(\mathrm{i}k_m z)\times \sum_{n=-\infty}^{n=+\infty}\left[\mathrm{H}(z-nL)-\mathrm{H}(z-b-nL)\right]. \quad (13)$$

The Heaviside step function summation was then written using a Fourier series as:

$$\sum_{n=-\infty}^{n=+\infty}\left[\mathrm{H}(z-nL)-\mathrm{H}(z-b-nL)\right] = -\sum_{n=-\infty}^{n=+\infty} d_n\exp\left(\frac{\mathrm{i}2\pi n z}{L}\right); \quad (14)$$

where

$$d_n=\begin{cases}\frac{1-\exp(-\mathrm{i}2\pi n b/L)}{\mathrm{i}2\pi n} & n\neq 0\\ \frac{b}{L} & n=0.\end{cases} \quad (15)$$

Equation. (14) was inserted into Eqs. (11), (12), and (13), which yielded:

$$\sum_{m=-\infty}^{m=+\infty}\sum_{q=0}^{q=+\infty}\left[\rho h c_p^2 k_m^2+\frac{\rho h c_p^2(1-\nu)q^2}{2a^2}-\rho h\omega^2\right]\times U_{mq}\cos(q\theta)\exp(\mathrm{i}k_m z)+ \sum_{m=-\infty}^{m=+\infty}\sum_{q=0}^{q=+\infty}\left[\frac{-\rho h c_p^2(1+\nu)\,\mathrm{i}\,k_m q}{2a}\right]\times V_{mq}\cos(q\theta)\exp(\mathrm{i}k_m z)+ \sum_{m=-\infty}^{m=+\infty}\sum_{q=0}^{q=+\infty}\left[\frac{-\rho h c_p^2 \nu\,\mathrm{i}\,k_m}{a}\right] W_{mq}\cos(q\theta)\exp(\mathrm{i}k_m z) = \frac{-K_z}{ab}\sum_{m=-\infty}^{m=+\infty}\sum_{q=0}^{q=+\infty} U_{mq}\cos(q\theta)\exp(\mathrm{i}k_m z)\times \sum_{n=-\infty}^{n=+\infty} d_n\exp\left(\frac{\mathrm{i}2\pi n z}{L}\right); \quad (16)$$

$$\sum_{m=-\infty}^{m=+\infty}\sum_{q=0}^{q=+\infty}\left[\frac{\rho h c_p^2(1+\nu)\,\mathrm{i}\,k_m q}{2a}\right]\times U_{mq}\sin(q\theta)\exp(\mathrm{i}k_m z)+ \sum_{m=-\infty}^{m=+\infty}\sum_{q=0}^{q=+\infty}\left[\frac{\rho h c_p^2(1-\nu)k_m^2}{2}+\frac{\rho h c_p^2 q^2}{a^2}-\rho h\omega^2\right]\times V_{mq}\sin(q\theta)\exp(\mathrm{i}k_m z)+ \sum_{m=-\infty}^{m=+\infty}\sum_{q=0}^{q=+\infty}\left[\frac{\rho h c_p^2\, q}{a^2}\right] W_{mq}\sin(q\theta)\exp(\mathrm{i}k_m z) = \frac{-K_t}{ab}\sum_{m=-\infty}^{m=+\infty}\sum_{q=0}^{q=+\infty} V_{mq}\sin(q\theta)\exp(\mathrm{i}k_m z)\times \sum_{n=-\infty}^{n=+\infty} d_n\exp\left(\frac{\mathrm{i}2\pi n z}{L}\right); \quad (17)$$

and

$$\sum_{m=-\infty}^{m=+\infty}\sum_{q=0}^{q=+\infty}\left[\frac{\rho h c_p^2 \nu \,\mathrm{i}\, k_m}{a}\right] U_{mq}\cos(q\theta)\exp(\mathrm{i}k_m z)+ \sum_{m=-\infty}^{m=+\infty}\sum_{q=0}^{q=+\infty}\left[\frac{\rho h c_p^2\, q}{a^2}\right] V_{mq}\cos(q\theta)\exp(\mathrm{i}k_m z)+ \sum_{m=-\infty}^{m=+\infty}\sum_{q=0}^{q=+\infty}\left[\frac{\rho h c_p^2}{a^2}+\frac{\rho h^3 c_p^2 k_m^4}{12}+\frac{\rho h^3 c_p^2 k_m^2 q^2}{6a^2}+ \frac{\rho h^3 c_p^2 q^4}{12a^4}-\rho h\omega^2\right] W_{mq}\cos(q\theta)\exp(\mathrm{i}k_m z) = P_a\exp(\mathrm{i}kz)-\frac{K_r}{ab}\sum_{m=-\infty}^{m=+\infty}\sum_{q=0}^{q=+\infty} W_{mq}\cos(q\theta)\exp(\mathrm{i}k_m z)\times \sum_{n=-\infty}^{n=+\infty} d_n\exp\left(\frac{\mathrm{i}2\pi n z}{L}\right). \quad (18)$$

The last term in Eqs. (16), (17), and (18) were rewritten using the relationships:

$$\sum_{m=-\infty}^{m=+\infty}\sum_{q=0}^{q=+\infty} U_{mq}\cos(q\theta)\exp(\mathrm{i}k_m z)\times \sum_{n=-\infty}^{n=+\infty} d_n\exp\left(\frac{\mathrm{i}2\pi n z}{L}\right) = \sum_{q=0}^{q=+\infty}\left\{\sum_{n=-\infty}^{n=+\infty}\sum_{m=-\infty}^{m=+\infty} U_{nq} d_{m-n}\exp(\mathrm{i}k_m z)\right\}\cos(q\theta); \quad (19)$$

$$\sum_{m=-\infty}^{m=+\infty}\sum_{q=0}^{q=+\infty} V_{mq}\sin(q\theta)\exp(\mathrm{i}k_m z)\times \sum_{n=-\infty}^{n=+\infty} d_n \exp\left(\frac{\mathrm{i}2\pi n z}{L}\right) = \sum_{q=0}^{q=+\infty}\left\{\sum_{n=-\infty}^{n=+\infty}\sum_{m=-\infty}^{m=+\infty} V_{nq} d_{m-n}\exp(\mathrm{i}k_m z)\right\}\sin(q\theta)\ ; \tag{20}$$

and

$$\sum_{m=-\infty}^{m=+\infty}\sum_{q=0}^{q=+\infty} W_{mq}\cos(q\theta)\exp(\mathrm{i}k_m z)\times \sum_{n=-\infty}^{n=+\infty} d_n \exp\left(\frac{\mathrm{i}2\pi n z}{L}\right) = \sum_{q=0}^{q=+\infty}\left\{\sum_{n=-\infty}^{n=+\infty}\sum_{m=-\infty}^{m=+\infty} W_{nq} d_{m-n}\exp(\mathrm{i}k_m z)\right\}\cos(q\theta)\ . \tag{21}$$

Equations (16) and (18) were then multiplied by $\exp(-\mathrm{i}k_s z)\cos(t\theta)$, Eq. (17) was multiplied by $\exp(-\mathrm{i}k_s z)\sin(t\theta)$, and these resulting expressions were integrated on the intervals $[0, 2\pi]$ on θ and $[0, L]$ on z. Because these functions were orthogonal on their respective domains, the equations decouple into sets of st-indexed equations. Each one was individually written as:

$$\left[\rho h c_p^2 k_s^2 + \frac{\rho h c_p^2(1-\nu)t^2}{2a^2} - \rho h\omega^2\right] U_{st} + \left[\frac{-\rho h c_p^2(1+\nu)\,\mathrm{i}\,k_s t}{2a}\right] V_{st} + \left[\frac{-\rho h c_p^2 \nu\,\mathrm{i}\,k_s}{a}\right] W_{st} = \frac{-K_z}{ab}\sum_{n=-\infty}^{n=+\infty} d_{s-n} U_{nt}\ ; \tag{22}$$

$$\left[\frac{\rho h c_p^2(1+\nu)\mathrm{i}\,k_s t}{2a}\right] U_{st} + \left[\frac{\rho h c_p^2(1-\nu)k_s^2}{2} + \frac{\rho h c_p^2 t^2}{a^2} - \rho h\omega^2\right] V_{st} + \left[\frac{\rho h c_p^2 t}{a^2}\right] W_{st} = \frac{-K_t}{ab}\sum_{n=-\infty}^{n=+\infty} d_{s-n} V_{nt}\ ; \tag{23}$$

and

$$\left[\frac{\rho h c_p^2 \nu\,\mathrm{i}k_s}{a}\right] U_{st} + \left[\frac{\rho h c_p^2 t}{a^2}\right] V_{st} + \left[\frac{\rho h c_p^2}{a^2} + \frac{\rho h^3 c_p^2 k_s^4}{12} + \frac{\rho h^3 c_p^2 k_s^2 t^2}{6a^2} + \frac{\rho h^3 c_p^2 t^4}{12a^4} - \rho h\omega^2\right] W_{st} = \frac{-K_r}{ab}\sum_{n=-\infty}^{n=+\infty} d_{s-n} W_{nt} + \begin{cases} P_a & s=t=0 \\ 0 & \text{otherwise.}\end{cases} \tag{24}$$

This equation were written in matrix form as:

$$\mathbf{A}(s,t)\mathbf{x}_{st} = \frac{-K_z}{ab}\sum_{n=-\infty}^{n=+\infty}\mathbf{Z}_{s-n}\mathbf{x}_{nt} + \frac{-K_r}{ab}\sum_{n=-\infty}^{n=+\infty}\mathbf{T}_{s-n}\mathbf{x}_{nt} + \frac{-K_r}{ab}\sum_{n=-\infty}^{n=+\infty}\mathbf{R}_{s-n}\mathbf{x}_{nt} + \begin{cases}\mathbf{f} & s=t=0\\ \mathbf{0} & \text{otherwise.}\end{cases} \tag{25}$$

The entries of the matrices and vectors in Eq. (25) are listed in the Appendix. The left-hand side of this equation represents the dynamics of the shell and the right-hand side represents the dynamics of the ring stiffeners acting on the shell and the external load applied to the shell. At this point, all of the axial (s) and radial (t) modes could be combined into a single global matrix and a solution to the wave propagation coefficients could be calculated. However, because the radial modes individually decoupled, it was numerically more efficient to solve each radial mode equation separately and then combine their individual solutions using Eqs. (5), (6), and (7). Eqation (25) was written for all values of s and any single value of t and combined into the matrix equation:

$$\hat{\mathbf{A}}\,\hat{\mathbf{x}} = \frac{-K_z}{ab}\hat{\mathbf{Z}}\,\hat{\mathbf{x}} - \frac{K_t}{ab}\hat{\mathbf{T}}\,\hat{\mathbf{x}} - \frac{K_r}{ab}\hat{\mathbf{R}}\,\hat{\mathbf{x}} + \hat{\mathbf{f}}. \tag{26}$$

In Eq. (26), using five s terms ($-2 \le s \le 2$) and any single t term, $\hat{\mathbf{A}}$ was a block diagonal matrix that contained the dynamics of the tth radial mode of the shell and was written as:

$$\hat{\mathbf{A}} = \begin{bmatrix} \mathbf{A}(-2,t) & \mathbf{0} & \mathbf{0} & \mathbf{0} & \mathbf{0} \\ \mathbf{0} & \mathbf{A}(-1,t) & \mathbf{0} & \mathbf{0} & \mathbf{0} \\ \mathbf{0} & \mathbf{0} & \mathbf{A}(0,t) & \mathbf{0} & \mathbf{0} \\ \mathbf{0} & \mathbf{0} & \mathbf{0} & \mathbf{A}(1,t) & \mathbf{0} \\ \mathbf{0} & \mathbf{0} & \mathbf{0} & \mathbf{0} & \mathbf{A}(2,t) \end{bmatrix}; \tag{27}$$

$\hat{\mathbf{Z}}$ was a rank deficient block partitioned matrix that represented the stiffener forces acting in the longitudinal direction on the shell and was written as:

$$\hat{\mathbf{Z}} = \begin{bmatrix} \mathbf{Z}_0 & \mathbf{Z}_{-1} & \mathbf{Z}_{-2} & \mathbf{Z}_{-3} & \mathbf{Z}_{-4} \\ \mathbf{Z}_1 & \mathbf{Z}_0 & \mathbf{Z}_{-1} & \mathbf{Z}_{-2} & \mathbf{Z}_{-3} \\ \mathbf{Z}_2 & \mathbf{Z}_1 & \mathbf{Z}_0 & \mathbf{Z}_{-1} & \mathbf{Z}_{-2} \\ \mathbf{Z}_3 & \mathbf{Z}_2 & \mathbf{Z}_1 & \mathbf{Z}_0 & \mathbf{Z}_{-1} \\ \mathbf{Z}_4 & \mathbf{Z}_3 & \mathbf{Z}_2 & \mathbf{Z}_1 & \mathbf{Z}_0 \end{bmatrix}; \tag{28}$$

$\hat{\mathbf{T}}$ was a rank deficient block partitioned matrix that represented the stiffener forces acting in the tangential direction on the shell and was written as:

$$\hat{\mathbf{T}} = \begin{bmatrix} \mathbf{T}_0 & \mathbf{T}_{-1} & \mathbf{T}_{-2} & \mathbf{T}_{-3} & \mathbf{T}_{-4} \\ \mathbf{T}_1 & \mathbf{T}_0 & \mathbf{T}_{-1} & \mathbf{T}_{-2} & \mathbf{T}_{-3} \\ \mathbf{T}_2 & \mathbf{T}_1 & \mathbf{T}_0 & \mathbf{T}_{-1} & \mathbf{T}_{-2} \\ \mathbf{T}_3 & \mathbf{T}_2 & \mathbf{T}_1 & \mathbf{T}_0 & \mathbf{T}_{-1} \\ \mathbf{T}_4 & \mathbf{T}_3 & \mathbf{T}_2 & \mathbf{T}_1 & \mathbf{T}_0 \end{bmatrix}; \tag{29}$$

$\hat{\mathbf{R}}$ was a rank deficient block partitioned matrix that represented the stiffener forces acting in the radial direction on the shell and was written as:

$$\hat{\mathbf{R}} = \begin{bmatrix} \mathbf{R}_0 & \mathbf{R}_{-1} & \mathbf{R}_{-2} & \mathbf{R}_{-3} & \mathbf{R}_{-4} \\ \mathbf{R}_1 & \mathbf{R}_0 & \mathbf{R}_{-1} & \mathbf{R}_{-2} & \mathbf{R}_{-3} \\ \mathbf{R}_2 & \mathbf{R}_1 & \mathbf{R}_0 & \mathbf{R}_{-1} & \mathbf{R}_{-2} \\ \mathbf{R}_3 & \mathbf{R}_2 & \mathbf{R}_1 & \mathbf{R}_0 & \mathbf{R}_{-1} \\ \mathbf{R}_4 & \mathbf{R}_3 & \mathbf{R}_2 & \mathbf{R}_1 & \mathbf{R}_0 \end{bmatrix}; \quad (30)$$

$\hat{\mathbf{f}}$ was the vector for the ring load that contained the system excitation and was equal to:

$$\hat{\mathbf{f}} = \{ \ \mathbf{0}^{\mathrm{T}} \quad \mathbf{0}^{\mathrm{T}} \quad \mathbf{f}^{\mathrm{T}} \quad \mathbf{0}^{\mathrm{T}} \quad \mathbf{0}^{\mathrm{T}} \ \}^{\mathrm{T}}; \quad (31)$$

$\hat{\mathbf{x}}$ was the vector of unknown wave propagation coefficients and was written as:

$$\hat{\mathbf{x}} = \{ \ \mathbf{x}_{-2,t}^{\mathrm{T}} \quad \mathbf{x}_{-1,t}^{\mathrm{T}} \quad \mathbf{x}_{0,t}^{\mathrm{T}} \quad \mathbf{x}_{1,t}^{\mathrm{T}} \quad \mathbf{x}_{2,t}^{\mathrm{T}} \ \}^{\mathrm{T}}; \quad (32)$$

where,

$$\mathbf{x}_{st} = \{ \ U_{st} \quad V_{st} \quad W_{st} \ \}^{\mathrm{T}}. \quad (33)$$

The three stiffness matrices from the ring stiffener could be combined into a single matrix, however, they were kept separate to facilitate an understanding of the dynamics of the system. Note from Eq. (26) that the ring stiffener's forces coupled the axial modes of the shell together and did not respond independently, like they would have if the shell had been unstiffened. The solution to the t indexed wave propagation coefficients in Eq. (26) were found by:

$$\hat{\mathbf{x}} = \left[\hat{\mathbf{A}} + \frac{K_z}{ab}\hat{\mathbf{Z}} + \frac{K_t}{ab}\hat{\mathbf{T}} + \frac{K_r}{ab}\hat{\mathbf{R}} \right]^{-1} \hat{\mathbf{f}}. \quad (34)$$

These were then inserted back into Eqs. (5), (6), and (7) to yield the displacement field of the shell at any location. The dispersion curves of the system were calculated using:

$$\det \left[\hat{\mathbf{A}} + \frac{K_z}{ab}\hat{\mathbf{Z}} + \frac{K_t}{ab}\hat{\mathbf{T}} + \frac{K_r}{ab}\hat{\mathbf{R}} \right] = 0; \quad (35)$$

Although the curves generated in the wavenumber-frequency space were typically too modally dense to fully understand the behavior of the free waves.

3. MODEL VERIFICATION AND CONVERGENCE CRITERIA

The model that was developed in Sections 2 was validated by comparing it to finite element analysis. In this example problem, the following cylinder parameters were used: Young's modulus $E = 1 \times 10^7$ Nm^{-2}, Poisson's ratio $\nu = 0.48$, density $\rho = 1200$ kgm^{-3}, radius $a = 0.1$ m, and thickness $h = 0.001$ m. Additionally, the following stiffener properties were used: periodicity $L = 5$ m, length $b = 0.5$ m, axial spring constant $K_z = 1.59 \times 10^5$ Nm^{-1}, and radial spring constant $K_r = 1.59 \times 10^5$ Nm^{-1}. The following loading parameters were used: axial wavenumber $k = 0$ and the magnitude of the applied pressure $P_a = 1$ Nm^{-2}. Figures 3 and 4 were the radial displacement and the longitudinal displacement of the shell at (top) 30 Hz, (middle) 60 Hz, and (bottom) 90 Hz versus spatial position. In these plots, the solid line was the analytical model created using 201 axial terms (max $|n| = 100$) and one radial term ($q = 0$) and the circular markers were the finite element models that used discrete springs to model the stiffener forces. The finite element results were produced using the COMSOL Multiphysics finite element program. This model consisted of an axisymmetric shell with a set of linear translational springs attached to the area between $z = 0$ and $z = b = 0.5$ m to mimic the behavior of the stiffener. This approach reduced the number of necessary degrees of freedom and allowed for an examination of the effect of mismatch between the spring and shell stiffness without the inclusion of inertial effects of the stiffener. The finite element model consisted of 20001 nodes, 20000 elastic axisymmetric continuum elements, 2000 translational springs in the radial direction, and 2000 translational springs in the longitudinal direction. By enforcing user defined pointwise constraints, the model was nodally constrained so that the behavior would be periodic on the interval $[0, L]$. The constraint expression between the terminal $[0, L]$ nodes was one of Floquet type periodicity, wherein the wavenumber relating their translational degrees of freedom was that of the applied excitation. There was no rotational spring constant, as the model was axisymmetric and the displacements in the angular direction were zero. A single radial term was sufficient to model the dynamics for this case because the excitation was a ring load. The displacement differences between the two models were almost zero at all longitudinal locations.

Convergence of the summations listed in Eqs. (5) to (7) was an open issue, as the rate of convergence was dependent on many of the model parameters. However, for the modeled system presented in this paper, several generalized statements could be made. The number of terms needed for convergence was directly related to the mismatch between the stiffness of the shell and the stiffness of the stiffeners. If the stiffeners were not present, then only a single term (the $n = 0$ and $q = 0$ term) was needed for the series to converge to the proper solution (for a ring load). The influence of the mismatch between the cylinder stiffness and the stiffener stiffness could be studied with respect to the convergence of the solution. Figure 5 was a plot of the radial displacement convergence of the system versus number of terms and frequency for stiffener constants of (a) $K_z = K_r = 1 \times 10^4$ Nm^{-1}, (b) $K_z = K_r = 1 \times 10^5$ Nm^{-1}, and (c) $K_z = K_r = 1 \times 10^6$ Nm^{-1}. This convergence metric was calculated using the equation:

$$C(N, f) = 20 \log_{10} \left[\frac{1}{J} \sum_{j=1}^{J} \left| \frac{W^C(x_j) - W^N(x_j)}{W^C(x_j)} \right| \right]; \quad (36)$$

where $W^C(x_j)$ was the radial displacement calculated using 401 axial terms for each series (max $|n| = 200$) and a single radial term ($q = 0$), $W^N(x_j)$ was the radial displacement

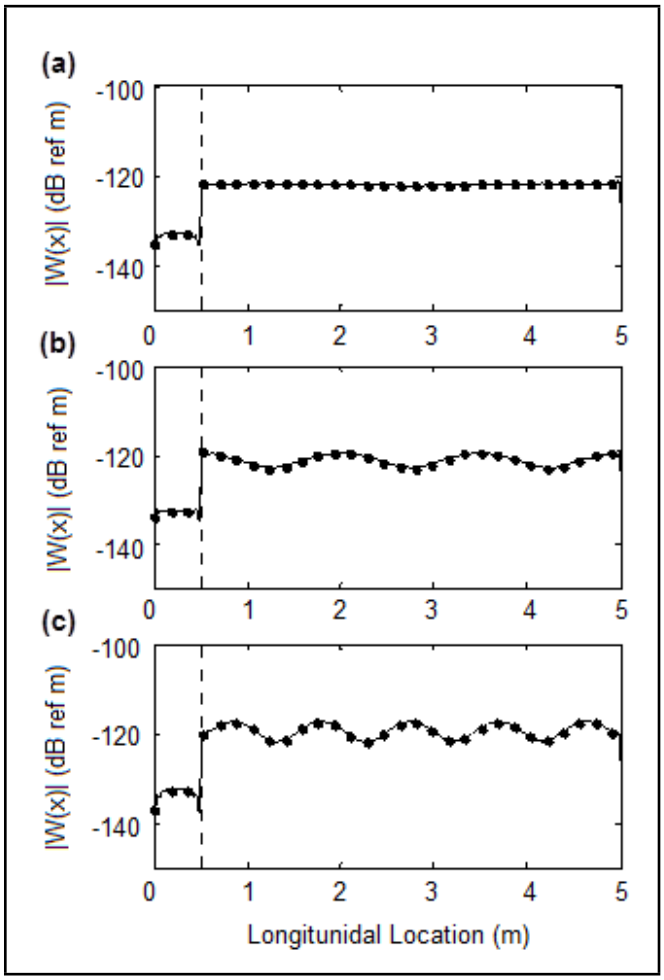

Figure 3. Radial displacement of the shell at (a) 30 Hz, (b) 60 Hz and (c) 90 Hz versus longitudinal location. The solid line is the analytical model and the circular markers are the finite element model with discrete springs modeling the stiffener. The dashed line $x = b = 0.5$ m denotes the location of the end of the stiffener.

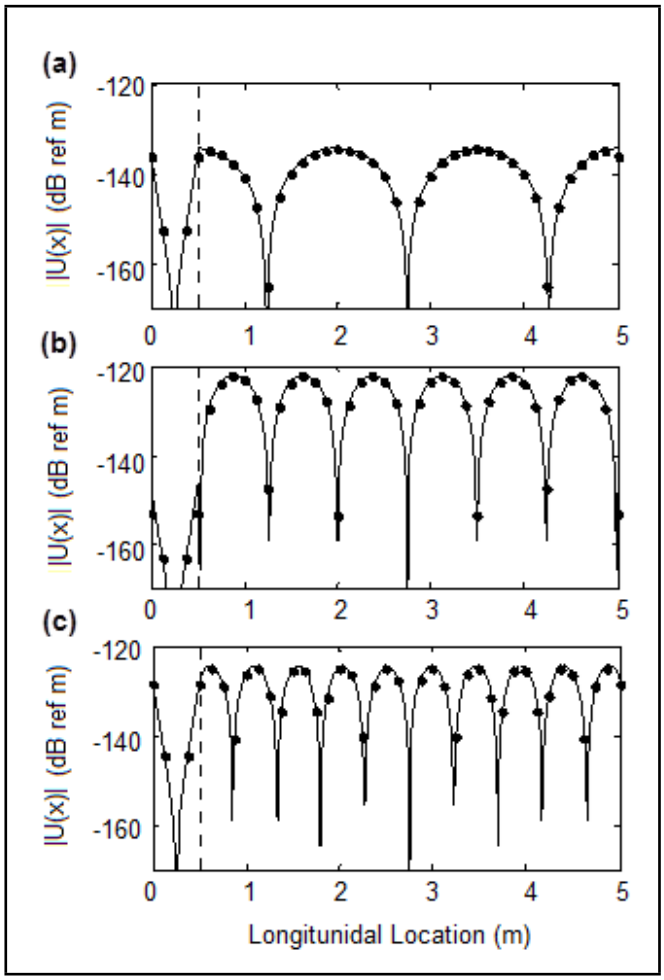

Figure 4. Longitudinal displacement of the shell at (a) 30 Hz, (b) 60 Hz and (c) 90 Hz versus longitudinal location. The solid line is the analytical model and the circular markers are the finite element model with discrete springs modeling the stiffener. The dashed line $x = b = 0.5$ m denotes the location of the end of the stiffener.

calculated using $2N + 1$ terms for each series, x_j was the location of the jth calculation, J was equal to 15, and the spatial locations were equally spaced from 0 to L. The region in white was -40 dB (or lower), which corresponded to a one percent (or less) normalized difference between the two solutions. As the ring stiffeners became stiffer, more terms were needed for the series to converge. It was useful to generate a plot similar to Fig. 5 in order to understand the decay of energy in the higher order terms and ensure convergence for any set of parameters that were to be modeled.

4. EXAMPLE PROBLEM USING AN INCIDENT PLANE WAVE LOAD

An example problem of system response to an incident plane wave load was then investigated. The cylinder parameters from Section 3 were used to calculate the displacement fields. For a plane wave load, the vector $\hat{\mathbf{f}}$ in Eq. (26) was equal to:

$$\hat{\mathbf{f}} = \{ \ \mathbf{0}^{\mathrm{T}} \quad \mathbf{0}^{\mathrm{T}} \quad \mathbf{f}_t^{\mathrm{T}} \quad \mathbf{0}^{\mathrm{T}} \quad \mathbf{0}^{\mathrm{T}} \quad \}^{\mathrm{T}}; \tag{37}$$

The entries of the vector in Eq. (37) are listed in the Appendix. The wave speed of the plane wave load was 343 ms^{-1} and the frequency of excitation is 60 Hz. Fig. 6 is a plot of the cylinder displacement in the (a) longitudinal direction, (b) the tangential direction, and (c) the radial direction versus spatial location z and angle θ using stiffness constants of the spacer parameters in Section 3, as this corresponded to a relatively soft elastomeric stiffener. The scale of the plot was in dB ref m. Figure 7 is a plot of the cylinder displacement in the (a) longitudinal direction, (b) the tangential direction, and (c) the radial direction versus spatial location z and angle θ using stiffness constants of $K_z = 2.46 \times 10^5$ Nm^{-1}, $K_t = 4.33 \times 10^5$ Nm^{-1}, and $K_r = 6.28 \times 10^5$ Nm^{-1}, which were derived from spacer properties of $E_S = 1.00 \times 10^8$ Nm^{-2}, $G_S = 3.45 \times 10^7$ Nm^{-2}, and $a_S = 0.0980$ m, $A_S = 0.0012$ m^2, $I_\theta = 1.18 \times 10^{-5}$ m^4, and $I_Z = 5.91 \times 10^{-6}$ m^4, using the approximations:

$$K_z \approx \frac{A_s E_s}{b}; \tag{38}$$

$$K_t \approx \frac{G_s I_\theta}{a_s^3}; \tag{39}$$

and

$$K_r \approx \frac{E_s I_z}{a_s^3}. \tag{40}$$

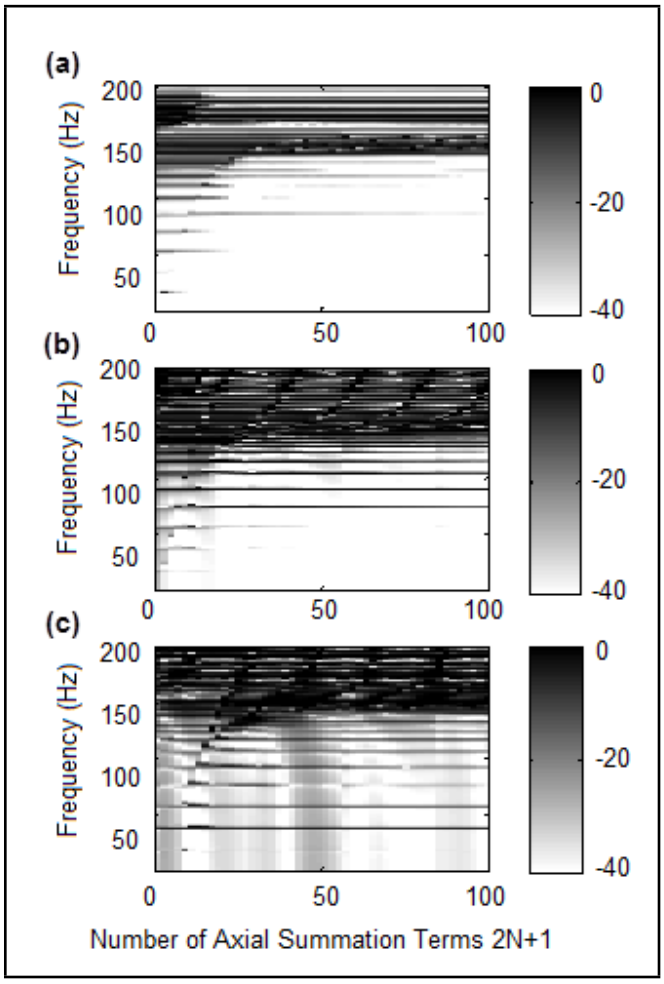

Figure 5. Convergence of the radial displacement versus total number of summation terms in each series and frequency for cylinder with periodic ring stiffeners expressed in a decibel scale. The stiffener constants used in the model were (a) $K_z = K_r = 1 \times 10^4$ Nm^{-1}, (b) $K_z = K_r = 1 \times 10^5$ Nm^{-1}, and (c) $K_z = K_r = 1 \times 10^6$ Nm^{-1}.

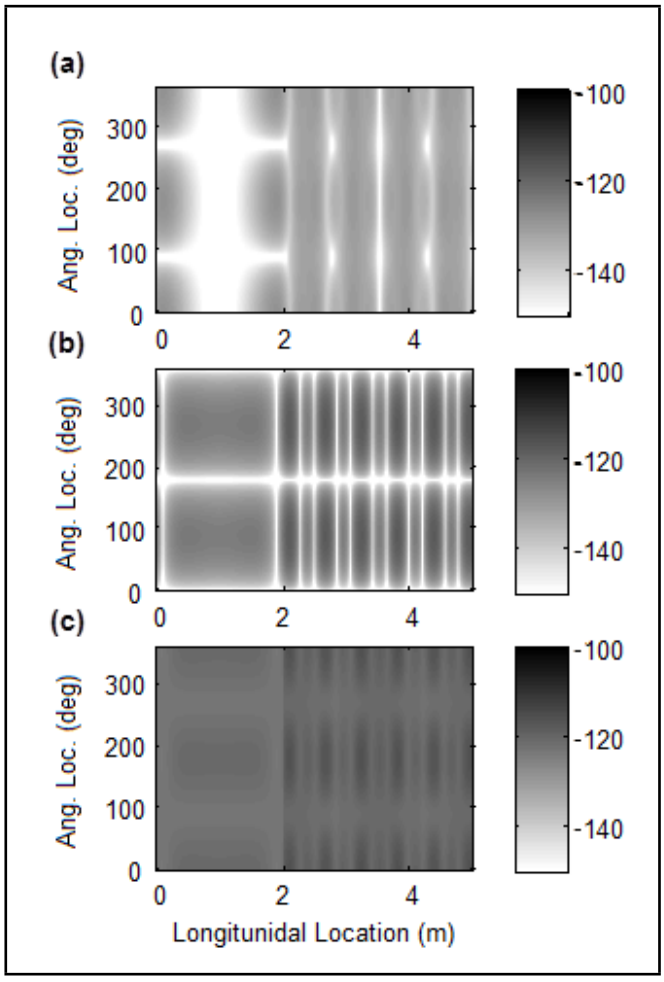

Figure 6. Displacement of the shell in the (a) longitudinal direction, (b) tangential direction and (c) radial direction modeled with a soft stiffener at 60 Hz versus longitudinal location and angular location. The scale of the plot is in dB ref m.

These values corresponded to a relatively hard elastomeric stiffener. The scale of the plot was in dB ref m. A comparison of Figs. 6 and 7 shows that as the stiffener value increased, the displacements had more spatial variation. Additionally, the effect of the hard stiffener was clearly discernable from 0 to 2.0 m in the displacement fields in Fig. 7, whereas it was less observable for the case of the soft stiffener. Figure 8 is a plot of the normalized magnitude of the (a) longitudinal coefficients, (b) tangential coefficients, and (c) radial coefficients versus longitudinal index s and tangential index t for the soft stiffener. Figure 9 is a plot of the normalized magnitude of the (a) longitudinal coefficients, (b) tangential coefficients, and (c) radial coefficients versus longitudinal index s and tangential index t for the hard stiffener. Because both of these plots were normalized, their scales were in dB. These plots were included so that the individual mode contributions could be discerned. Note that the higher order modes for the system with the hard stiffener had more energy than the system with the soft stiffener. Numerical simulations suggested that when the values of the higher order modes were approximately 80 dB below the value of the maximum mode, the displacement summations converged. One final note was that if the external load was some form other than a normal ring load or plane wave, then its analytical form had to be transformed into a series solution and inserted into the right hand side of Eq. (22) for longitudinal excitation, Eq. (23) for tangential excitation, and Eq. (24) for radial excitation.

5. CONCLUSIONS

This paper has derived a model of an infinite length cylindrical shell with finite length and periodically spaced ring stiffeners. Using a dynamic formulation of the Donnell shell equations, the stiffener effects are included as forces on the right hand side of the longitudinal, tangential, and radial equations of motion using Heaviside step functions. The displacements are then written as double summations with unknown coefficients multiplied by a tangential and a longitudinal function. These are inserted into the equations of motion and the Heaviside functions are replaced with their Fourier series representations. These equations are then orthogonalized on both the angular and longitudinal domains, resulting in sets of algebraic double indexed equations. These equations are assembled into a global matrix equation and the result is a solution to the displacement fields. Two example problems are included and dis-

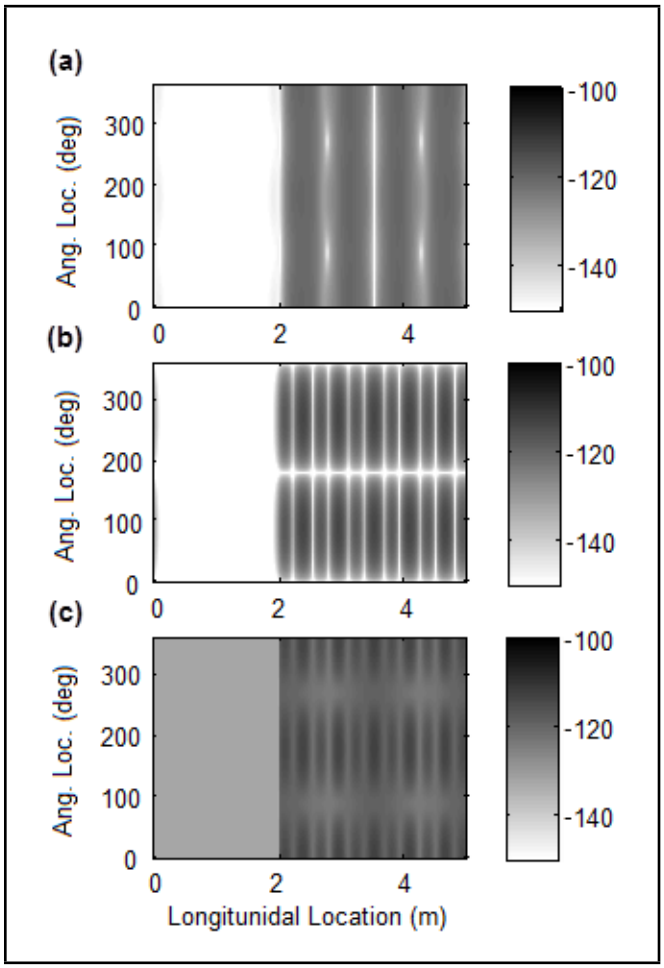

Figure 7. Displacement of the shell in the (a) longitudinal direction, (b) tangential direction and (c) radial direction modeled with a hard stiffener at 60 Hz versus longitudinal location and angular location. The scale of the plot is in dB ref m.

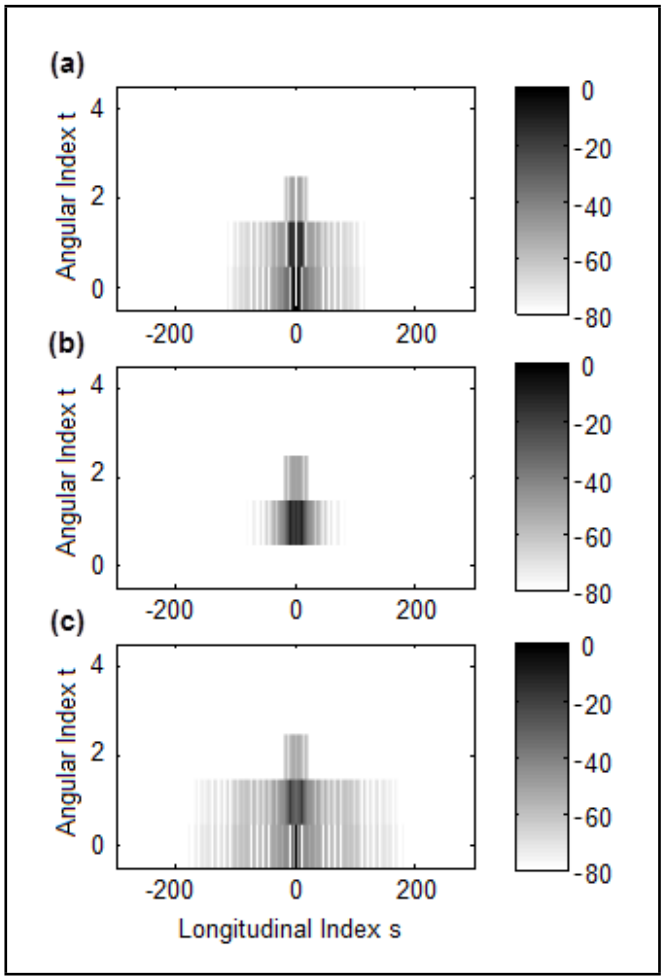

Figure 8. Normalized magnitude of the (a) longitudinal coefficients, (b) tangential coefficients and (c) radial coefficients versus longitudinal index and angular index for the soft stiffener. The scale of the plot is in dB.

cussed: the system subjected to a ring load and the system subjected to a plane wave. The ring load example is verified with finite element results. The problem of varying the stiffness of the stiffeners is studied and the corresponding changes in the shell displacements are examined. Finally, the modal distribution of the displacement field and convergence of the double summations is discussed.

ACKNOWLEDGEMENTS

This paper was funded by the Naval Undersea Warfare Center's In-House Laboratory Independent Research Program.

REFERENCES

[1] Graf, K. F. *Wave Motion in Elastic Solids,* Dover Publications, New York, New York (1975).

[2] Junger, M. C. and Feit, D. *Sound, Structures, and Their Interaction,* MIT Press, Cambridge, Massachusetts (1986).

[3] Gazis, D. C. Three-dimensional investigation of the propagation of waves in hollow circular cylinders. *I. Analytical foundation, J. Acoust. Soc. Am.,* **31** (5), 568–573, (1959). http://dx.doi.org/10.1121/1.1907753

[4] Ding, H., Chen, W., and Zhang, L. *Elasticity of Transversely Isotropic Materials,* Springer, Netherlands, (2006) http://dx.doi.org/10.1007/1-4020-4034-2

[5] Peloquin, M. S. Forced harmonic vibration of the generally orthotropic cylindrical shell with inner and outer fluid loading, Naval Undersea Warfare Center Technical Report 10,199, New London, Connecticut, (1992).

[6] Bennett, M. S. and Accorsi, M. L. Free wave propagation in periodically ring stiffened cylindrical shells, *Journal of Sound and Vibration,* **171** (1), 49–66, (1994). http://dx.doi.org/10.1006/jsvi.1994.1103

[7] Al-Najafi, A. M. J. and Warburton, G. B. Free vibration of ring-stiffened cylindrical shells, *J. Sound Vib.*, **13** (1), 9–25, (1970). http://dx.doi.org/10.1016/s0022-460x(70)80076-1

[8] Jafari, A. A. and Bagheri, M. Free vibration of non-uniformly ring stiffened cylindrical shells using analytical, experimental and numerical methods, *Thin-Walled Struct.*, **44** (1), 82–90, (2006). http://dx.doi.org/10.1016/j.tws.2005.08.008

[9] Beskos, D. E. and Oates, J. B. Dynamic analysis of ring-stiffened circular cylindrical shells, *J. Sound Vib.*,

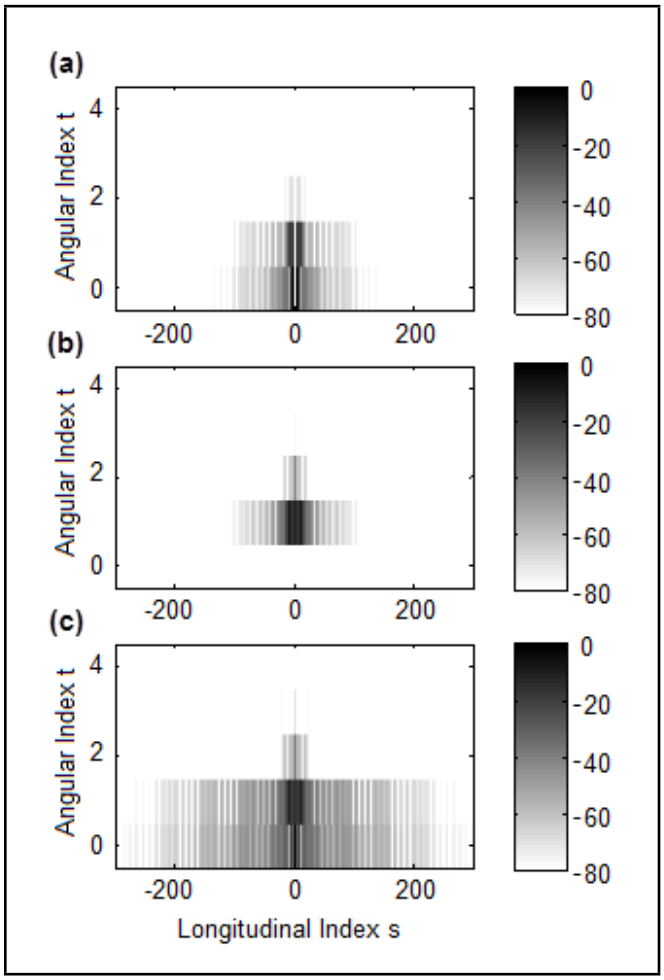

Figure 9. Normalized magnitude of the (a) longitudinal coefficients, (b) tangential coefficients and (c) radial coefficients versus longitudinal index and angular index for the hard stiffener. The scale of the plot is in dB.

75 (1), 1–15, (1981). http://dx.doi.org/10.1016/0022-460x(81)90232-7

[10] Burroughs, C. B. Acoustic radiation form fluid-loaded infinite circular cylinders with doubly periodic ring supports, *J. Acoust. Soc. Am.*, **75** (3), 715–722, (1984). http://dx.doi.org/10.1121/1.390582

[11] Hodges, C. H. Power, J. and Woodhouse, J. The low frequency vibration of a ribbed cylinder, Part 1: theory, *J. Sound Vib.*, **101** (2), 219–235, (1985). http://dx.doi.org/10.1016/s0022-460x(85)81217-7

[12] Mead, D. J. and Bardell, N. S. Free vibration of a thin cylindrical shell with periodic circumferential stiffeners, *J. Sound Vib.*, **115** (3), 499–520, (1987). http://dx.doi.org/10.1016/0022-460x(87)90293-8

[13] Gan, L., Li, X., and Zhang, Z. Free vibration analysis of ring-stiffened cylindrical shells using wave propagation approach, *J. Sound Vib.*, **326** (3–5), 633–646, (2009). http://dx.doi.org/10.1016/j.jsv.2009.05.001

[14] Pan, Z., Li, X., and Ma, J. A study on free vibration of a ring-stiffened thin circular cylindrical shell with arbitrary boundary conditions, *J. Sound Vib.*, **314** (1–2), 330–342, (2008). http://dx.doi.org/10.1016/j.jsv.2008.01.008

APPENDIX — MATRIX AND VECTOR ENTRIES

The entries of the matrices and vectors in the text are listed below. The entries of $\mathbf{A}(s,t)$ in Eq. (25) are

$$a_{1,1} = \rho h\omega^2 - \rho h c_p^2 k_s^2 - \frac{\rho h c_p^2 (1-\nu) t^2}{2a^2}; \tag{A.1}$$

$$a_{1,2} = \frac{-\rho h c_p^2 (1+\nu) k_s t}{2a}; \tag{A.2}$$

$$a_{1,3} = \frac{\rho h c_p^2 \nu \, \mathrm{i} k_s}{a}; \tag{A.3}$$

$$a_{2,1} = \frac{-\rho h c_p^2 (1+\nu) k_s t}{2a}; \tag{A.4}$$

$$a_{2,2} = \rho h\omega^2 - \frac{\rho h c_p^2 (1-\nu) k_s^2}{2} - \frac{\rho h c_p^2 t^2}{a^2}; \tag{A.5}$$

$$a_{2,3} = \frac{\rho h c_p^2 \, \mathrm{i} t}{a^2}; \tag{A.6}$$

$$a_{3,1} = \frac{\rho h c_p^2 \nu \, \mathrm{i} k_s}{a}; \tag{A.7}$$

$$a_{3,2} = \frac{\rho h c_p^2 \, \mathrm{i} t}{a^2}; \tag{A.8}$$

and

$$a_{3,3} = \frac{\rho h c_p^2}{a^2} + \frac{\rho h^3 c_p^2 k_s^4}{12} + \frac{\rho h^3 c_p^2 k_s^2 t^2}{6a^2} + \frac{\rho h^3 c_p^2 t^4}{12a^4} - \rho h\omega^2. \tag{A.9}$$

The non-zero entry of $\mathbf{Z}_m$ in Eq. (28) is

$$z_{1,1} = d_m. \tag{A.10}$$

The non-zero entry of $\mathbf{T}_m$ in Eq. (29) is

$$t_{2,2} = d_m. \tag{A.11}$$

The non-zero entry of $\mathbf{R}_m$ in Eq. (30) is

$$r_{3,3} = d_m. \tag{A.12}$$

The non-zero entry of $\mathbf{f}$ in Eq. (25) is

$$f_{3,1} = P_a. \tag{A.13}$$

The non-zero entry of $\mathbf{f}_t^T$ in Eq. (37) is

$$\mathbf{f}_t^{\mathrm{T}} = \left\{ \begin{array}{cc} 0 & 0 \end{array} \quad P_a \, \mathrm{i}^t \varepsilon_t \, \mathrm{J}_t \left(\tfrac{\omega c}{a}\right) \right\}^{\mathrm{T}}. \tag{A.14}$$